Available online at www.sciencedirect.com
SCIENCE DIRECT®
Polymer 44 (2003) 4735–4745
polymer
www.elsevier.com/locate/polymer

Motion and sorption of gas molecules in poly(octadecyl acrylate)

David Zanuy[a], D. Alfonso Zazueta[b], Carlos Alemán[b,*]

[a]*Laboratory of Experimental and Computational Biology, NCI-Frederick, Bldg. 469, Rm. 147, Frederick, MD 21702, USA*
[b]*Departament d'Enginyeria Química, E.T.S. d'Enginyers Industrials de Barcelona, Universitat Politècnica de Catalunya, Diagonal 647, Barcelona E-08028, Spain*

Received 17 October 2002; received in revised form 16 May 2003; accepted 16 May 2003

Abstract

Monte Carlo simulations are reported on the sorption and motion of small gas molecules (CH_4 and CO_2) in poly(octadecyl acrylate), a typical comb-like polymer with biphasic structure. Calculations were performed using a computational procedure recently developed by us, which is suitable to simulate the motion and sorption of small molecules in dense comb-like polymers. To our knowledge, the problem of gas transport in comb-like polymers using explicit penetrant molecules is for the first time studied by computational techniques. The study involves more than 12 million Monte Carlo steps of systems constituted by more than 1470 explicit atoms/pseudoatoms. Solubility coefficients are discussed by comparison with recently reported experimental data.

Keywords: Comb-like polymers; Gas sorption; Monte Carlo simulations

1. Introduction

The biphasic structure of comb-like polymers, in particular of poly(*n*-alkyl-(meth)acrylate)s [1–6], poly(γ-*n*-alkyl-α-glutamate)s [7–10], and poly(α-*n*-alkyl-β-aspartate)s [7,11–14], has been a subject of interest by both experimental and theoretical researches for the last decades. These systems are constituted by flexible side chains, i.e. long linear alkyl groups, attached to a main chain with a stiff helical conformation. The biphasic organization of comb-like polymers typically consists of a layered arrangement of main chain helical rods separated by a paraffinic inter-phase.

It has been found that the structure of the paraffinic inter-phase greatly depends on the temperature. Thus, at low temperatures the side-chains pack in a hexagonal crystal structure (phase A). However, a thermally-induced phase transition related with the melting of the crystallized side chains occurs after heating above a transition temperature (T_o). In this new phase, usually denoted as phase B, the side chains are in a disordered state while the main chains retain the initial layered arrangement. It should be emphasized that in phase B the paraffinic chains stand more or less aligned in a elongated conformation but not in an actual molten state [6,12–14]. Fig. 1 shows the sketch of a typical phase transition in comb-like polymers.

The phase B of comb-like polymers could be considered as a particular case of semi-crystalline systems. However, there is a fundamental difference between conventional semi-crystalline polymers and comb-like polymers: in the former materials, the chemical composition of the crystal and amorphous phases is identical, whereas in the latter compounds the rigid main chain and the side chains usually present chemical differences. Thus, many properties of comb-like polymers depend on not only the backbone stiffness and the organization of the paraffinic inter-phase but also on the chemical differences between them. Among these properties the gas-sorption and transport have become a topic of increasing interest in the last five years since dramatic changes are expected upon traversing the melting point of the side chains [13,15–17].

In a very recent work, Mogri and Paul [16,17] investigated the gas sorption and transport in poly(octadecyl acrylate), henceforth abbreviated PA-18. Results revealed an increase of the solubility and the transport coefficients, which are penetrant dependent, at the melting point of the side chains. This switch was explained by the immobilization of the side chains when the temperature (T) is lower than T_o. Thus, at $T < T_o$ (phase A) the crystallized paraffinic phase forms an impenetrable barrier to

* Corresponding author. Tel.: +34-934016681; fax: +34-934016600.
E-mail address: carlos.aleman@upc.es (C. Alemán).

0032-3861/03/$ - see front matter © 2003 Elsevier Science Ltd. All rights reserved.
doi:10.1016/S0032-3861(03)00403-8

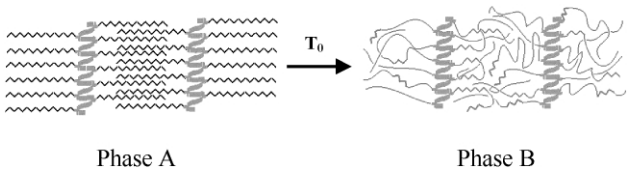

Fig. 1. Typical phase transition in comb-like polymers.

permeation since a tortuous path for the penetrants is created. Conversely, the melting of the side chains at $T > T_o$ (phase B) reduces the tortuosity for the diffusion of the gas molecules in the inter-phase. This is consistent with the earliest concept [18] about gas diffusion in semi-crystalline materials: the crystalline phase acts as barrier against diffusion while the amorphous represents a sorbing and permeable phase. However, classical two-phase models [19,20] based in such concepts are not able to completely describe the gas diffusion in PA-18 [16,17]. Presumably, this is due to the chemical differences between the organized main chains, which include an ester group, and the paraffinic phase [17].

Many questions about the gas sorption and transport in comb-like polymers remain unanswered up to date. Some of these need work on the atomistic scale. However, it is not possible to get direct experimental data at these dimensions. Over the last two decades detailed atomistic computational methods have become a powerful tool for the investigation of gas sorption and diffusion in amorphous and crystalline materials [21–24]. Unfortunately, the atomistic simulation of partially ordered multichain dense polymer systems, like comb-like polymers, is extremely difficult [6]. Thus, standard computational methods, like molecular dynamics or Metropolis Monte Carlo (MC), either become impractical or lead to poor results.

It is the aim of this work to provide some results and additional interpretations concerning the motion and solubility of gas molecules in comb-like polymers. For this purpose, we have explored the sorption and diffusion of CH_4 and CO_2 penetrants in PA-18 using an advanced and efficient MC sampling technique, which has been recently developed to study comb-like polymers [6]. We have concentrated our efforts in the phase B of PA-18 since, as was discussed above, it can be considered as a reduced model of the semi-crystalline state.

2. Computational methods

2.1. PA-18 representation

Isotactic PA-18 was modeled with eight independent chains, each of them constituted by eight explicit residues. The main chains were arranged in a 2/1 helical conformation as was observed by X-ray diffraction [25]. The values for the dihedral angles ξ_1 and ξ_2 (Fig. 2(a)) were generated using a procedure previously developed by us

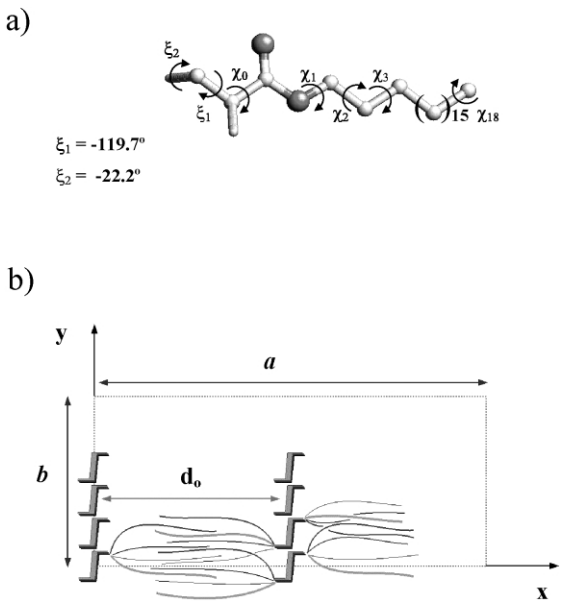

Fig. 2. (a) Atomistic representation of the residue for PA-18. Torsion parameters (in degrees) along backbone helix and alkyl side chains are indicated. (b) Schematic representation of the simulation box used in MC simulations. The view is along the helix axis (z-axis) and only the side chains of some parent helices are presented.

[26]. This is based on a corrected grid search algorithm, which was designed to built all the molecular arrangements sterically allowed compatible with a given helical symmetry and an axial repeat length. The resulting dihedral angles, $\xi_1 = -119.7°$ and $\xi_2 = -22.2°$ [6], were kept fixed during the simulations, which is consistent with the experimental observation for the phase B of PA-18 [25,27]. The helices were initially packed in an orthorhombic box of dimensions $a = 60.00$ Å, $b = 22.00$ Å and $c = 15.43$ Å, and with the helix axis oriented parallel to the z-axis. The y-axis was defined as pointing along the line joining centers of neighboring helices within a layer. The x-axis pointed, therefore, perpendicular to the layers and helix layers were parallel to the y–z plane. A schematic representation of the simulation box used in the calculations is displayed in Fig. 2(b).

There is some ambiguity regarding the sense of the helices in the molecular packing [25,27]. However, this is not expected to influence the results of our simulations because: (i) the helices are constituted by non-polar atoms; and (ii) the interlayer distance, which is symbolized by d_o in Fig. 2(b), is very large [27]. Accordingly, the chains were arranged parallel with respect to each other. Periodic boundary conditions were applied along the three axes by using the minimum image convention.

A united-atom approximation was used for the CH, CH_2 and CH_3 groups, i.e. a description using pseudoatoms. The resulting system contains a total of 1472 atoms/pseudoatoms. Bond lengths and angles were kept fixed at the values reported in the Amber libraries [28,29].

2.2. Penetrants representation

The CH_4 was described using a spherical pseudoatom while an explicit model with three atoms was used for CO_2. The main characteristics of these penetrants are displayed in Table 1. Simulations were performed considering N gas molecules ($N = 5, 10, 15$ and 20), which were randomly introduced into the simulation box. A separation among the different gas molecules larger than 10 Å was the only restriction imposed in this procedure. In this way the distribution of the penetrant molecules into the polymeric matrix was homogeneous.

2.3. Simulation details

All the MC simulations were performed using our last version of the MCDP/2 [6] computer program. The side chains of comb-like PA-18 were sampled using the configurational bias (CB) algorithm [30,31], which consists of the following three steps: (i) a chain is selected at random; (ii) the chain is cut at a random position; and (iii) the chain is sequentially re-grown bond-by-bond by examining a number of positions (N_s), which are chosen randomly. The CB method was adapted to simulate tethered chains, which is the situation encountered in comb-like polymers, i.e. the side chains are attached to a core defined by the main chain conformation [32]. In addition to CB-MC moves, a small fraction of Metropolis moves (15–20%) was also used for side chains.

In a first stage, simulations of NVT and NPT types were performed for isolated PA-18, i.e. without penetrants, at $P = 1$ atm and $T = 325$ K. This temperature was identified by Mogri and Paul as the transition temperature T_o for the melting of the alkyl side chains in PA-18 (see Fig. 1) [16]. In the CB algorithm, a total of $N_s = 8$ torsion angles were used to sample torsional space for side chains. The degrees of freedom in simulations were: (i) the setting angles of the 2/1 helices; (ii) the conformation of the alkyl side groups; (iii) the volume of the simulation box (only in NPT simulations). The frequencies used for these types of MC moves in both NVT and NPT simulations are listed in Table 2.

The last recorded microstructure of PA-18 simulations was used to insert the penetrants according to the procedure described above. Thus, in a second stage simulations of NPT and NVT types were carried out at the same pressure and temperature for PA-18 with penetrants. These simulations will be denoted, henceforth, PA-18 + $N$$CH_4$ and PA-18 + $N$$CO_2$. In addition to those indicated for PA-18, the positions of the penetrant molecules within the simulation box were also considered as degrees of freedom, which were moved according to the following sequence. First, a penetrant is selected at random. Second, for CO_2, i.e. a non-spherical penetrant, the type of movement, translational or rotational, is randomly selected. Third, the penetrant is moved from the old position to the new one using the Metropolis algorithm. Details about these simulations are provided in Table 2. It should be noted that the consideration of such types of moves, as a whole, implies that the gas molecules follow a diffusive regime through the polymeric matrix. This is fully consistent with the experimental observations reported for PA-18 [16]. Thus, a switch in the diffusion coefficients of CH_4 and CO_2 was detected when phase A transformed into phase B indicating a dependence with the density and the free volume.

The Amber force-field was used to represent the van der Waals and torsional energies of the system [28,29]. The van der Waals energy was computed in the usual pair-wise additive way using a Lennard-Jones 6-12 potential. The van der Waals parameters, σ and ϵ, were computed using arithmetic and geometric mean combining rules, respectively. Electrostatic interactions were neglected for the system by the following two reasons: (i) the ester groups, which are the most charged ones, have a very low mobility since they are directly attached to the main chain helices, (ii) the mobile alkyl side chains can be considered as electrically neutral. Furthermore, the variations observed in the transport and solubility coefficients when phase A transforms into phase B are due to the changes in the organization of the paraffinic pool [16]. On the other hand, previous studies considering different polymers and penetrants revealed a linear correlation of the logarithm of the Henry's law constant with Lennard-Jones well-depth [33], which justifies the omission of atomic charges in CO_2. This trend indicates that CO_2 can be represented using a simple Lennard-Jones potential, such model being able to provide excellent results [34,35].

Nonbonding interactions were truncated at 12 Å. A three-term Fourier series expansion was used to represent the torsional energy. Nonbonding and torsional parameters for PA-18 were taken from Amber libraries [28,29] while parameters for CH_4 and CO_2 are displayed in Table 1.

Table 1
van der Waals (R and ϵ in Å and kcal/mol, respectively) parameters used to describe the CH_4 and CO_2 penetrants

Atom	R	ε
CH_4	1.909	0.294
C (CO_2)[a]	1.85	0.120
O (CO_2)[a]	1.60	0.20

[a] The O = C bond length used to built the CO_2 molecule was 1.162 Å.

3. Results and discussion

3.1. The Structure of PA-18

Simulations on PA-18 were reported in a very recent work [6]. Thus, this system was used to check the performance of the MCDP/2 computer code. However, in order to improve the understanding of our results for PA-18 + $N$$CH_4$ and

Table 2
Number of steps and frequency (in %) for the different types of Monte Carlo moves in simulations of PA-18 without and with penetrant molecules

System	#	Type	No. of Steps (equil)[a]	No. of Steps (prod)[b]	CB[c]	Metrop.[c]	a/b[d]	θ[e]	Penetrant[f]
PA-18	1	NVT	1×10^5	–	70	15	–	15	–
	2	NPT	1.75×10^5	1.75×10^5	55	15	15	15	–
	3	NVT	1×10^5	2×10^5	70	15	–	15	–
PA-18 + NCH$_4$ $N = 5, 10, 15, 20$	4	NPT	1×10^5	3×10^5	25	5	25	15	30
PA-18 + NCO$_2$ $N = 5, 10, 15, 20$	5	NPT	1×10^5	3×10^5	25	5	25	15	30
PA-18 + 10CH$_4$	6	NVT	1×10^5	4×10^6	30	5		15	50
PA-18 + 10CO$_2$	7	NVT	1×10^5	4×10^6	30	5		15	50

[a] Length of the equilibration period.
[b] Length of the production run.
[c] Frequency of CB and Metropolis moves for the alkyl side chains.
[d] Frequency of NPT moves: a/b corresponds to the dimensions of the simulation box.
[e] Frequency of moves for the setting angles.
[f] Frequency of moves for the penetrants.

PA-18 + NCO$_2$, we decided to include here a brief report summarizing the most important features.

In order to relax the unfavorable interactions created by the overlap of the alkyl side chains in the initial arrangement, a MC simulation consisting of 1.0×10^5 steps of NVT type was run (simulation #1 in Table 2). The last microstructure of such simulation was used as starting point of a new simulation of NPT type, which consisted of 3.5×10^5 steps (simulation #2 in Table 2). The lattice parameters equilibrate at $a = 65.8$ Å and $b = 31.2$ Å, which correspond to an expansion of about 10 and 30%, respectively, with respect to the initial values. These data are consistent with the available experimental information, as indicates the good agreement between the experimental, $d_o = 32$ Å [27], and predicted interlayer distances, $d_o = a/2 = 32.9$ Å.

Next, a new simulation of NVT type consisting of 3×10^5 steps (simulation #3 in Table 2) was performed using as starting point the lattice dimensions and the atomic coordinates of the previous NPT simulation. The results allowed characterize the structure and conformation of the alkyl side chains. For this purpose atomic coordinates were saved every 2×10^3 steps during the last 2×10^5 steps, which was considered as the production phase. Fig. 3(a) shows a population analysis for the dihedral angles, χ_i, of the side chain. As can be seen, the *trans* is the most populated state for all the dihedral angles with exception of χ_{11}, which prefers a *skew* conformation. Moreover, the frequency of occurrence of the *trans* conformation is larger than 72% for six dihedral angles. It should be noted that the conformational distribution displayed in Fig. 3(a) is a mixture of those expected for phases A and B. Thus, previous studies in other comb-like polymers indicated that the population of *trans* is around 85–100% in the phase A [36], while in the phase B it decreases to about 60–65% [12–14].

On the other hand, Fig. 3(b) shows the normalized radial distribution functions computed for methylene pseudoatoms of different residues ($g_{\text{int-res}}(r)$) and different chains ($g_{\text{int-ch}}(r)$), respectively. As can be seen, both $g_{\text{int-res}}(r)$ and $g_{\text{int-ch}}(r)$ present a broad peak at around 4.6 Å, which is close to the distance between two paraffinic chains when crystallize in a hexagonal lattice [37]. Again, these results should be considered as a mixture of those expected for phases A

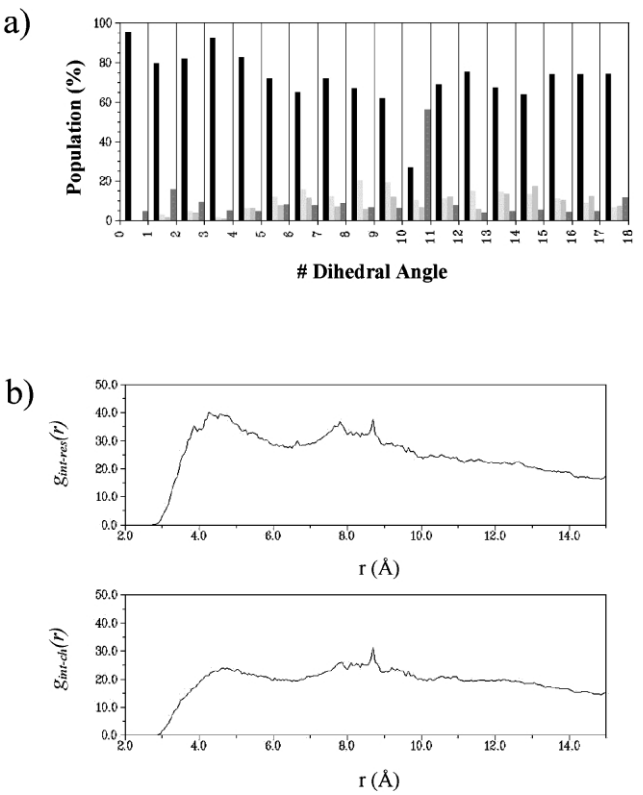

Fig. 3. (a) Population analysis of the torsional angles associated with each of the 18 bonds in the alkyl side chains of pure PA-18 (simulation #3 in Table 2). The four categories displayed for each bond, in the order displayed in the figure from left to right, are: *trans*, *gauche* $^+$, *gauche* $^-$ and the remaining conformers. (b) Inter-residue ($_{\text{gint-res(r)}}$) and inter-chain ($_{\text{gint-ch(r)}}$) pair distribution functions for methylene groups of side chains in PA-18 (simulation #3 in Table 2).

and B. In the former phase a sharp peak, rather than a broad one, appears at 4.6 Å indicating that a large number of methylene groups are involved in the hexagonal crystal of the paraffinic inter-phase [36]. However, the distribution functions obtained for phase B were almost identical to that of liquid C_{18} [14].

In summary, the results displayed in Fig. 3 indicate that the paraffinic chains present a small degree of crystallization. This is a very reasonable behavior since, as was mentioned before, simulations were performed at the transition temperature T_o and, therefore, paraffinic chains in crystallized and melted states should coexist. On the other hand, recent studies have proved that the computational method used in this work satisfactorily reproduces the order-disorder thermal transitions of comb-like polymers [38]. Accordingly, it should be considered that Fig. 3 provides a good description of comb-like PA-18.

3.2. Simulations of NPT type for PA-18NCH$_4$ and PA-18NCO$_2$

In order to study the influence of the penetrant molecules in the dimensions of the simulation box, MC simulations of NPT type (simulation #4 and #5 in Table 2) were performed for PA-18 + NCH$_4$ and PA-18 + NCO$_2$, N being 5, 10, 15 and 20. For this purpose, penetrant molecules were randomly inserted in the last microstructure recorded for PA-18. The length of each run was of 4×10^5 steps and, in all cases, the parameters a and b remained almost constant through the simulation. Thus, the lattice dimensions resulting from these simulations were very similar to those obtained for PA-18 indicating that influence of the penetrants is negligible. The parameters obtained from the average of the values recorded in the last 1×10^5 steps of the production runs were $a = 65.6$ Å and $b = 31.9$ Å, which were used subsequently in simulations of NVT type to study the motion of the CH_4 and CO_2 molecules through the polymeric matrix.

3.3. Simulations of NVT type for PA-18 + 10CH$_4$ and PA-18 + 10CO$_2$

3.3.1. Motion of the gas molecules

The motion of gas molecules through PA-18 was investigated in detail considering $N = 10$ (simulations #6 and #7 in Table 2). For this purpose, we used the box dimensions obtained in the previous section, which were maintained constant along the simulation. The system was equilibrated for a length of 1×10^5 steps. It should be noted that the frequency of the penetrant moves was fixed to 50% (Table 2) increasing the efficiency of the sampling. After this the energy of the system was completely equilibrated and a production run consisting of 4×10^6 steps was performed, the atomic coordinates being saved every 2×10^3 steps.

Fig. 4 represents the distribution of the distances between the penetrant molecules and the closest helix layer (d). The values of d range from 0 (helix layer) to ~16 Å (center of the paraffinic inter-phase). Sharp and well-defined peaks appear at small values of d, i.e. around 3–4 Å, indicating a remarkable tendency of the CH_4 and CO_2 penetrants to be in the regions near to the layers. Furthermore, the position of the maximum is about 1 Å smaller for CO_2 than for CH_4. After this, a broad distribution appears along the whole paraffinic phase for the CH_4 penetrants, whereas for CO_2 the distribution becomes more pronounced at the center of the paraffinic inter-phase.

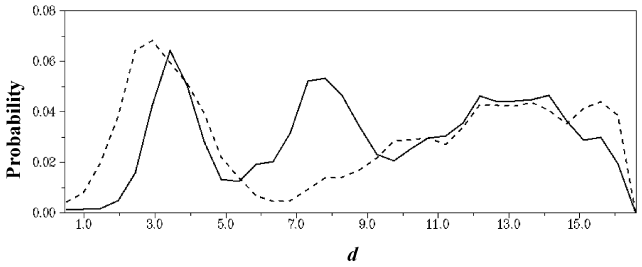

Fig. 4. Distribution of the distances between the CH_4 (continuous line) and CO_2 (dashed line) penetrants and the helix layer (d, in Å). The layer and the center of the paraffinic inter-phase are located at 0 at 16.4 Å, respectively.

One of the major aims of this work is to analyze the simulations in terms of the type of motions that the penetrants undergo. Fig. 5(a) shows the displacement with respect to the initial position after equilibration, $R(\#) = |r(\#) - r(0)|$ for representative CH_4 and CO_2 molecules. It should be mentioned that a very similar behavior was found for the remaining gas molecules. These results provide qualitative information about the walk of the penetrants through the polymeric matrix. As it can be seen, two different types of motion are identified. Over a relatively

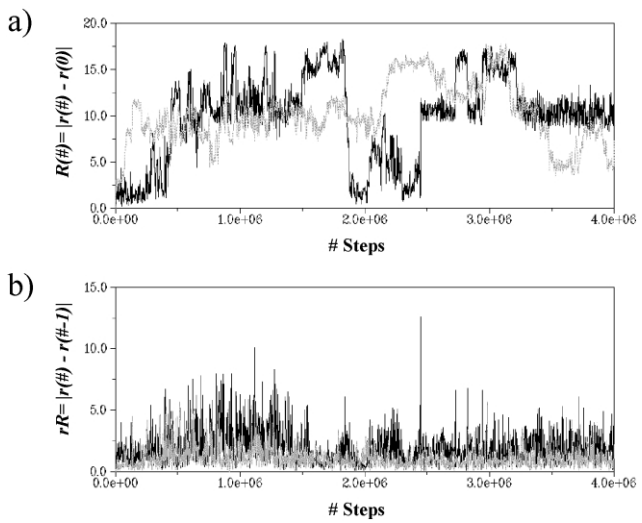

Fig. 5. (a) Displacement (in Å), $R(\#) = |r(\#) - r(0)|$ of representative CH_4 (black) and CO_2 (gray) molecules from its origin in the PA-18 matrix as a function of the simulation MC steps. (b) Displacement (in Å), $rR(\#) = |r(\#) - r(\# - 1)|$, of representative CH_4 (black) and CO_2 (gray) molecules between two consecutive MC steps. The peaks correspond to jumps among cavities. Results correspond to simulations #6 and #7 in Table 2.

high number of steps (typically 1×10^5–3×10^5 steps) the penetrant molecules explore the unoccupied space of the cavities that contain them. However, sometimes the gas molecules jump from one cavity to another following a hopping mechanism. These long-range movements determine the diffusive motion of the penetrants in the polymeric matrix. These features are clearly illustrated in Fig. 6, which shows the path followed by representative gas molecules through the polymeric matrix.

Fig. 5(b) displays the relative displacement, $rR(\#) = |r(\#) - r(\# - 1)|$, i.e. the displacement between two consecutive steps. A measure of the diffusive jumps, which are defined as a change in the positions of the penetrants from one cavity to the other, is provided by the larger values of $rR(\#)$. As can be seen, jumps are larger and more frequent for CH_4 than for CO_2. These differences can be explained considering the shape and size of the penetrants. Thus, CH_4 was represented as a small Lennard-Jones sphere whereas CO_2 was described using an explicit three-atoms model. As a result rR values of even 12 Å were obtained for CH_4 while the largest value achieved for CO_2 was about 6 Å.

On the other hand, inspection to the displacements in the Cartesian directions x, y and z, indicated that the jumps between different cavities generally occur along well defined directions. For both penetrants, the hopping between cavities mainly occurs in the continuous paraffinic interphase, i.e. the y and z directions in Fig. 2. Thus, the layers of parallel helices act as an obstacle confining the penetrants within the paraffinic regions. The frequency of penetrant movement through the layers was investigated by examining the stored configurations. In average, CH_4 and CO_2 molecules cross the layer after about 8.7×10^5 and 1.2×10^6 steps, respectively, which represents a very low frequency. The displacement of the penetrant molecules through the (x, y) plane (see Fig. 2) has been represented in Fig. 7, the position of the helix layers being indicated by continuous gray lines. As can be seen, the movement of CH_4 and CO_2 molecules across the layers of helices is rather uncommon. A detailed inspection of the recorded microstructures reveals that the displacement through the layers takes place along the channels located between neighboring helices. These transient channels are very narrow due to the minimum interchain distances. An atomistic picture showing the motion of a gas molecule through a helix layer is displayed in Fig. 8.

Overall the results indicates that the biphasic structure of comb-like PA-18 induces a large diffusional anisotropy. As usual in amorphous polymers [21], hopping events are facilitated in the paraffinic inter-phase by transitient channels of unoccupied volume between existing cavities. The formation of such channels is due to the thermal motions of the host polymer atoms in a low-density phase. However, the creation of channels in the plane of the layer is very difficult due to the efficient packing of rigid helices produces.

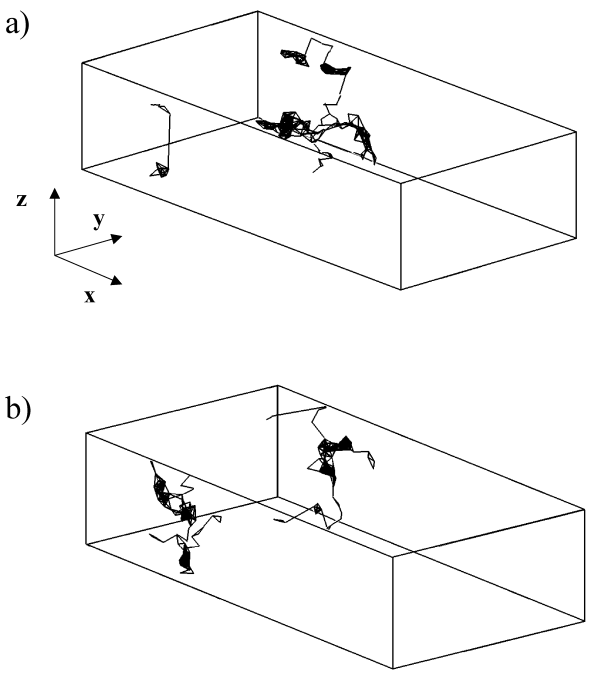

Fig. 6. Diffusion trajectories for representative CH_4 (a) and CO_2 (b) molecules in PA-18 (simulations #6 and #7 in Table 2). The x-, y- and z-axes have been indicated.

3.3.2. Structure of the polymeric matrix and examination of the unoccupied space

The influence of the gas molecules in the structure of the paraffinic region was examined by analyzing the results provided by simulations #6 and #7. Fig. 9 shows the population analyses of dihedral angles χ_i obtained for the PA-18 + 10CH_4 and PA-18 + 10CO_2 systems. Comparison with results displayed in Fig. 3(a) suggests that the gas molecules do not alter the preference for the *trans* conformation. Indeed, the only difference appears in the

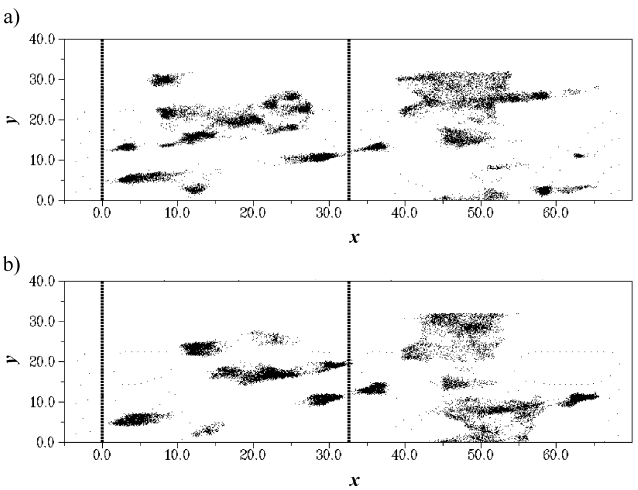

Fig. 7. Displacement (in Å) of the CH_4 (a) and CO_2 (b) penetrant molecules through the (x, y) plane (see Figure 2) of the simulation box (simulations #6 and #7 in Table 2). Continuous thick lines indicate the positions of the helix layers.

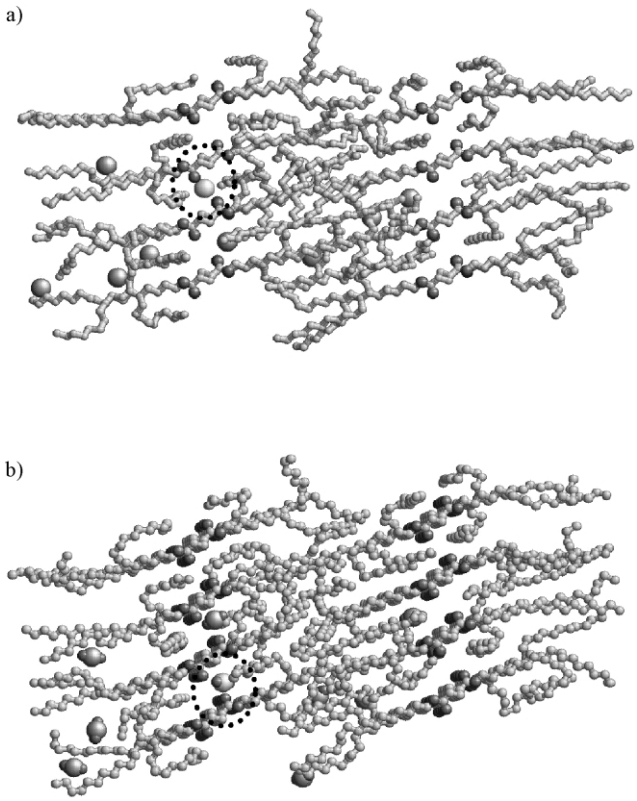

Fig. 8. Projection along the z-axis of microstructures obtained from (a) PA-18 + $10CH_4$ and (b) PA-18 + $10CO_2$ simulations (#6 and #7 in Table 2) showing the motion of the penetrants through the helix layers. Dashed circles mark representative gas molecules crossing the helix layers.

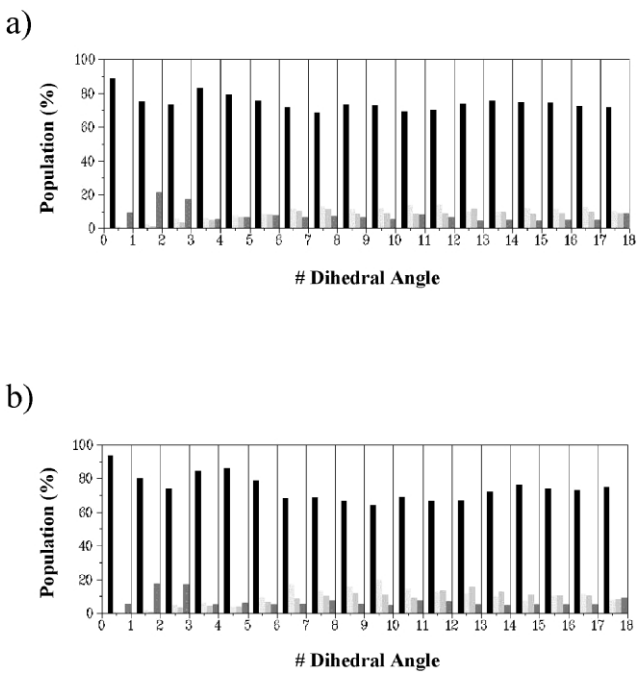

Fig. 9. (a) Population analysis of the torsional angles associated with each of the 18 bonds in the alkyl side chains of (a) PA-18 + $10CH_4$ (simulation #6 in Table 2) and (b) PA-18 + $10CO_2$ (simulation #7 in Table 2). The four categories displayed for each bond, in the order displayed in the figure from left to right, are: *trans*, *gauche* $^+$, *gauche* $^-$ and the remaining conformers.

population of χ_{11}, which change from *skew* to *trans*. On the other hand, no significant difference was found between the results obtained for the PA-18 + $10CH_4$ and PA-18 + $10CO_2$, the largest variation in the populations being 7%. The radial distribution functions $g_{\text{int-res}}(r)$ and $g_{\text{int-ch}}(r)$ derived from simulations with $N = 10$ were almost identical to that displayed in Fig. 3(b). Analyses of simulations #4 and #5 with $N = 5, 15$ *and* 20 neither provide deviations with respect to the behavior detected for PA-18.

In order to check if the change in χ_{11} is physically significant, we performed some additional simulations of PA-18 using different initial configurations, i.e. configurations obtained from simulations #6 and #7 were used as starting points after removing the penetrant molecules. Results (data not shown) were fully consistent with those displayed in Fig. 9 indicating that the difference found in χ_{11} is consequence of the initial configuration. According to these data, it can be concluded that the motion of small gas molecules does not exert any significant influence in the structure of the polymeric matrix. This behavior agrees with the accepted theories of gas motion. Thus, the 'jumping' model postulates an independent movement for both gas particle and polymeric matrix, allowing a diffusive event only when internal polymer motion randomly creates a new cavity [22].

The unoccupied volume (V_u) concept, i.e. the volume not

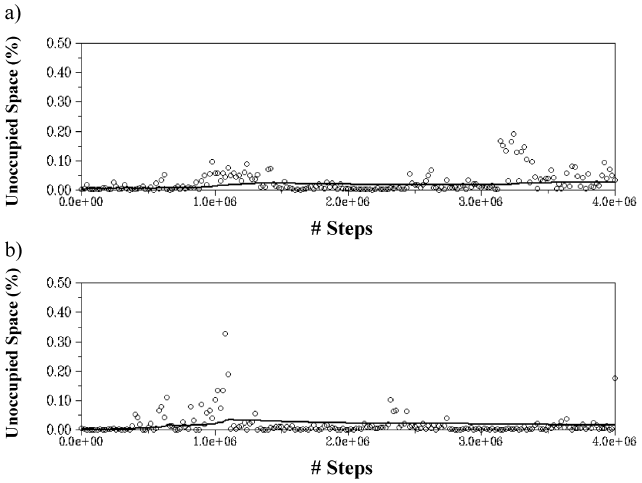

Fig. 10. Convergence of the unoccupied space (in %) for the CH_4 (a) and CO_2 (b) penetrants (simulations #6 and #7 in Table 2).

occupied by the atoms of the polymeric matrix that is accessible to a particle of given dimensions, has been widely invoked in interpreting the motion of the penetrant molecules. V_u was estimated for the systems under study using the microstructures recorded from simulations #6 and #7. For this purpose, the simulation box was divided into a three-dimensional uniformly spaced grid. A grid spacing of 0.5 Å was considered [24], the grids consisting of 285285 nodes. Then, the V_u for the spherical penetrant was evaluated using a simple procedure. A CH_4 molecule was centered in each node and the distance to the nearest atom of the polymeric matrix was measured. If this distance was larger than the sum of the van der Waals radii of the penetrant and the polymer atom, the node was identified as unoccupied. The linear shape of the CO_2 molecule was taken into account using a three steps procedure. First, the nodes accessible to the carbon atom were identified. Second, for each accessible node the oxygen atoms were added using the bond length displayed in Table 1. After this, a total of 12 orientations were considered for each CO_2 molecule, which correspond to those that can be defined in a cubic mesh if the carbon atom is located at the center of a cube. Then, for each orientation the steric clashes between the CO_2 molecule and the polymer matrix were evaluated using the corresponding van der Waals radii. If no steric clash was identified in at least one orientation, the node accessible to the carbon atom was considered as unoccupied.

The V_u averaged over the 2000 stored microstructure was 0.026 and 0.034% for CH_4 and CO_2, respectively. Fig. 10 shows the progress of V_u for the generated microstructures. Each point corresponds to the V_u measured for one microstructure (for clarification of the figure only 200 values spaced by 2×10^4 steps have been represented), while the solid lines display the mean values of V_u up to this microstructure. It is worth noting that, in general, the points present small deviations with respect to the lines drawn. The extremely low values of V_u reinforce the idea recently proposed by Mogri and Paul [16]: the gas transport in comb-like polymers can be controlled by the transition temperature T_o. Thus, phase A transform into phase B after reach T_o producing an increase in the mobility of the flexible alkyl groups.

3.3.3. Excess chemical potential and solubility

The infinite-dilution excess chemical potentials of CH_4 and CO_2 penetrants sorbed in PA-18 microstructures were calculated using the following expression

$$\beta\mu_i^{ex}(\rho, T) = -\ln\langle e^{-\beta\phi}\rangle_N \quad (1)$$

where $\beta = 1/k_bT$, ϕ is the interaction energy between the penetrant particle and the N particles of the system, and $\mu_i^{ex}(\rho, T)$ is the excess chemical potential of species i at temperature T and number density $\rho = N/V$. Two related but independent procedures were used to estimate μ_i^{ex}, which were the Widom's insertion and deletion methods [39,40]. In the former method μ_i^{ex} is calculated from the change in the potential energy caused by the insertion of a test-particle at a given random position. In order to improve the efficiency of this procedure we have centered a penetrant particle only in those regions where successful insertions are more likely to occur, i.e. the nodes identified as unoccupied in the previous section and the nodes occupied by the 10 explicit penetrants. Within this framework the ensemble average is defined as [41]

$$\langle\exp(-\beta\phi)\rangle = \sum_{j=1}^{Ne}(1/N_{T,j}) = \sum_{i=1}^{Nvj}\exp(-\beta\phi_i) \quad (2)$$

where N_{vj} is the number of sites without overlaps in the microstructure j, N_{Tj} is the total number of insertions for a given microstructure j assuming a uniform insertion density, and N_e is the total number of microstructures available for computing the ensemble of averages. The rotation of the CO_2 molecule was considered by applying the following strategy. Once the unoccupied grid points were identified using the procedure described above, we generated the twelve pre-selected orientations for the CO_2 molecule, i.e. those associated to a carbon atom surrounded by an 'oxygen cube'. Then, the energy of each possible orientation was evaluated providing the interaction energy between the penetrant molecule and the polymer matrix. The energy associated to the insertion of a CO_2 molecule in each unoccupied node was expressed as the weighted average of the calculated energies.

On the other hand, μ_i^{ex} was also computed using the Widom's deletion method, in which a penetrant particle is removed from the PA-18 + $10CH_4$ and PA-18 + CO_2 systems. The main disadvantage of the deletion method originates from the fact that each particle can only be removed once from the system, which could led to poorly converged averages for systems with low values of N. However, this should be compensated by the large number of steps considered in simulations #6 and #7.

Table 3
CH_4 and CO_2 excess chemical potentials (kcal/mol) and both predicted and experimental solubility coefficients (cm^3(STP)/cm^3 atm) for PA-18. The ratio of the solubility (S_{CH_4}/CO_2) coefficients of the two gases investigated are also displayed for comparison

	Widom's insertion	Widom's deletion	Experimental[a]
$\mu^{ex}_{CH_4}$	0.140	0.317	–
$\mu^{ex}_{CO_2}$	−0.910	−1.259	–
$S(CH_4)$	0.68	1.39	0.2
$S(CO_2)$	2.90	6.06	0.8
S_{CH_4/CO_2}	0.23	0.23	0.2

[a] Taken from Ref. [16].

Fig. 11 shows the progress of μ_i^{ex} ($i = CH_4$ *and* CO_2) for the 2000 generated microstructures computed by both the insertion and deletion methods. Each symbol corresponds to one application of Eq. (1) to one of the microstructures recorded from MC simulations (in order to clarify the figure symbols have been represented for microstructures spaced by 2×10^4 steps). It is worth noting that the mean values of μ_i^{ex}, which are represented by lines, are running over the symbols indicating the convergence of the simulations.

Table 3 shows the average values of μ_i^{ex} obtained for the two penetrants. As can be seen there is a qualitative agreement between the results provided by the insertion and deletion methods. Thus, a repulsive interaction between the CH_4 penetrant and the polymeric matrix is predicted by the two procedures, whereas an attractive interaction is obtained for the CO_2 penetrant. However, the strength of repulsive interaction provided for CH_4 is slightly overestimated by the deletion method with respect to the insertion one. A different situation appears for CO_2 since the deletion method overestimates the strength of the favorable interaction by 0.35 kcal/mol. This discrepancy is probably due to the predominance of the configurations with attractive interaction energies in the deletion method, which leads to systematic diminishment of μ_i^{ex}.

The calculated values of μ_i^{ex} were used to evaluate the solubility, S_o, which is defined as the concentration of the gas in a volume element of the polymer that is in equilibrium with the outside gas at a given pressure. Thus, S_o is related with μ_i^{ex} by the following equation

$$S_o = e^{-\mu^{ex}/RT} \tag{3}$$

The relation between S_o and the experimental solubility coefficient, S, in a unit of cm^3(STP)/cm^{-3} atm is written by

$$S = \left(\frac{T_o}{TP_o}\right) S_o \tag{4}$$

where $T_o = 273.15$ K, T is the temperature of the system and $P_o = 1$ atm.

The values predicted for S are compared with the experimental data [16] in Table 3. It should be emphasized that experimental data belongs to the molten state and, therefore, caution is required for this comparison. The results achieved by both the Widom's insertion and deletion algorithms are in qualitative agreement with experimental values. Thus, both methods predict that $S(CO_2)$ is larger than $S(CH_4)$, even although the former coefficient is overestimated. As often reported, S can be related with the condensability of the gas as measured by the critical temperature, normal boiling point, or more commonly the Lennard-Jones potential-well depth [42]. The more condensable is the gas, the more soluble is it. In other words, the relatively high boiling point of CO_2 is responsible for the

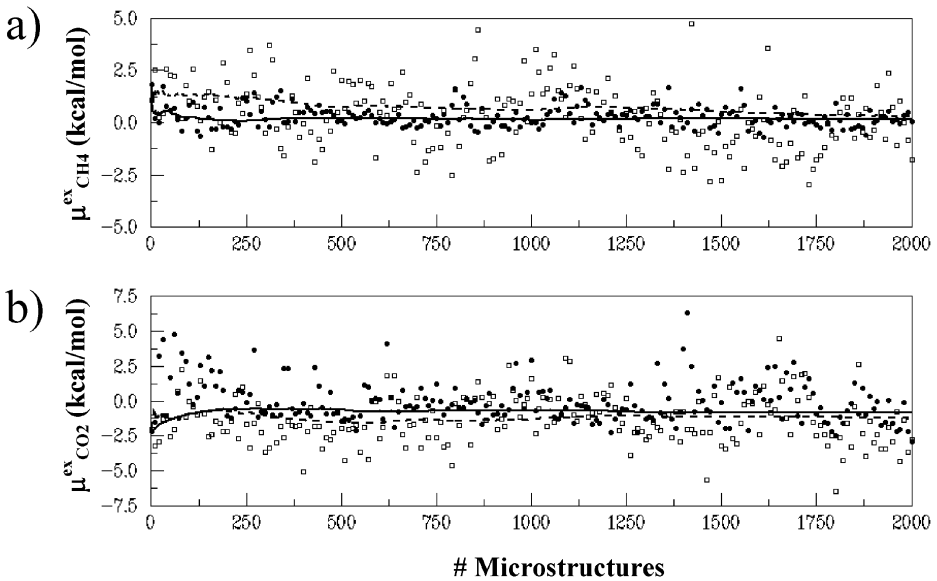

Fig. 11. Convergence of the excess chemical potential (in kcal/mol) of (a) CH_4 and (b) CO_2 calculated using the Windom's insertion method (black dots and solid lines) and the Widom's deletion method (empty squares and dashed lines) in the microstructures obtained from simulations #6 and #7 (Table 2).

high solubility of this gas in PA-18 in comparison with that of CH_4. As shown in Table 3, $S(CO_2)$ is predicted to be about a factor of 4 larger than $S(CH_4)$ by the two Widom's schemes, this difference being also detected experimentally. This agreement is reflected in Table 3, which includes the ratio of the solubility coefficients of the two gases investigated, S_{CH_4/CO_2}. Accordingly, the values predicted by the two methods (0.23) are in excellent agreement with the experimental value (0.2).

3.3.4. Diffusion

The diffusion coefficient, D, can be obtained in principle from diffusion trajectories of penetrant molecules within the polymeric matrix determined during Molecular Dynamics (MD) simulations. Thus, on long time scale the motion of a gas molecule can be described by the Einstein relation [43]:

$$6Dt = \langle |r(t) - r(0)|^2 \rangle \tag{5}$$

with $t \rightarrow \infty$, where $r(t)$ denotes the position of the center of mass of the gas molecule at the time t and $\langle \ldots \rangle$ represents the average over all gas molecules and over all averaging time origins. Moreover, some strategies as the Transition State Approach (TSA), have been developed in order to evaluate D from MC simulations [22]. The TSA approach assumes that: (i) the penetrants move in the polymeric matrix by thermally activated jumps; and (ii) on the times scales relevant for the penetrant transport the polymer atoms only eleastically fluctuate about certain average. Accordingly, the properties of the penetrants are described with a time-independent single-particle distribution function. However, this complex approach, which involves a number of additional assumptions that must be justified in each case, provides results that are usually in poor quantitative concordance with experimental data.

In order to provide a rough estimation of the transport coefficients, we have used a very approximate but simple strategy. Accordingly, Eq. (5) was employed by combining the mean-square displacements derived from MC simulations with the D values determined by Mogri and Paul [16], 5×10^{-6} and 6×10^{-6} $cm^2\ s^{-1}$ for CH_4 and CO_2, respectively. This allowed establish a relation between the evolution of the MC simulations, in terms of MC steps, and the time scale. The data obtained for PA18 + 10CH_4 were used to predict the coefficient for CO_2, while the coefficient for CH_4 was found from the relation for PA18 + 10CO_2. Furthermore, only the last 1×10^6 MC steps were used in this procedure, assuming that a diffusive regime has been reached after several millions of MC steps. The predicted diffusion coefficients were 2×10^{-7} and 1×10^{-7} cm^2/s for CH_4 and CO_2, respectively. The theoretical estimations are systematically underestimated with respect to the experimental data by an order of magnitude. Obviously, this discrepancy is consequence of the simplicity of our approach. However, these results indicate that both $D(CH_4)$ and $D(CO_2)$ are very similar, which is in qualitative agreement with the experimental measures.

4. Summary

In this work, we have discussed the behavior of CH_4 and CO_2 gas molecules in the biphasic PA-18 matrix. Results have been obtained using an advanced algorithm especially developed for the simulation the motion of small rigid particles in comb-like polymers [6]. Comparison among the results provided by simulations of pure PA-18, PA-18 + N CH_4 and PA-18 + $N$$CO_2$ showed that the biphasic structure of the polymeric matrix remains essentially unaltered by the motion of the gas molecules.

The Widom's insertion and deletion methods were used to estimate μ^{ex} and S. The results provided by the former method were very close to experimental data while the latter one tends to overestimate such parameters. However, both algorithms correctly predict that $S(CO_2) > S(CH_4)$ since the interactions of the polymer matrix with the CO_2 penetrants are attractive whereas those with CH_4 are slightly repulsive. However, perhaps even more important that the possible prediction of qualitative sorption coefficients is that the computational tools implemented in MCDP/2 permit deeper insight into comb-like polymers, which cannot be investigated using traditional simulation methods.

Acknowledgements

The authors are greatly indebted to the Centre Europeu de Parallelisme de Barcelona (CEPBA) for computational facilities. This work was supported by DGICYT with grant No. 3QU20000990.

References

[1] Platé NA, Shibaev VP, Petrukhin BS, Zubov YA, Kargin VA. J Polym Sci: Part A 1971;9:2291.
[2] Hsieh HWS, Post B, Morawetz H. J Polym Sci: Polym Phys 1976;14:1241.
[3] Beiner M, Schröter K, Hempel E, Reissig S, Donth E. Macromolecules 1999;32:6278.
[4] Platé NA, Shibaev VP. Comb-shaped polymers and liquid crystals. New York: Plenum Press; 1987.
[5] Alig I, Jarek M, Hellmann GP. Macromolecules 1998;31:2245.
[6] León S, Zanuy D, Alemán CJ. Comput Chem 2002;23:685.
[7] Loos K, Muñoz-Guerra S. In: Ciferri A, editor. Supramolecular polymers. New York: Marcel Dekker; 2000. p. 263–321.
[8] Watanabe J, Ono H, Uematsu I, Abe A. Macromolecules 1985;18:2141.
[9] Daly WH, Negulescu II, Russo PS, Poche DS. In: Shoever P, Balazs AC, editors. Macromolecular assemblies in polymer systems. ACS symposium series no. 493; 1992. p. 292–9.
[10] Watanabe J, Takashina Y. Macromolecules 1991;24:3423.

[11] López-Carrasquero F, Montserrat S, Martínez de Ilarduya A, Muñoz-Guerra S. Macromolecules 1995;28:5535.
[12] Muñoz-Guerra S, López-Carrasquero F, Alemán C, Morillo M, Castelleto V, Hamley I. Adv Mater 2002;14:203.
[13] Zanuy D, Alemán C, López-Carrasquero F, Báez ME, García-Álvarez M, Laso M, Muñoz-Guerra S. Macromol Chem Phys 2001;202:564.
[14] León S, Alemán C, Muñoz-Guerra S, Laso MJ. Theor Comput Polym Sci 2000;10:177.
[15] Compañ V, Zanuy D, Andrio A, Morillo M, Alemán C, Muñoz-Guerra S. Macromolecules 2002;35:4521.
[16] Mogri Z, Paul DR. Polymer 2001;42:2531.
[17] Mogri Z, Paul DR. J Polym Sci 2001;39:979.
[18] Michaels AS, Bixler HJ. J Polym Sci 1961;50:413.
[19] Petropoulus JH. J Polym Sci: Polym Phys 1985;23:201.
[20] Cussler EL, Hughes SE, Ward WJ, Aris R. J Membr Sci 1988;38:161.
[21] For a recent review see Hofmann D, Fritz L, Ulbrich J, Schepers C, Böhning M. Macromol Theory Simul 2000;9:293.
[22] Gusev AA, Müller-Plate F, van Gunsteren WF, Suter UW. Adv Polym Sci 1994;116:207.
[23] Müller-Plathe FJ. Chem Phys 1995;103:4346.
[24] Zanuy D, León S, Alemán C, Muñoz-Guerra S. Polymer 2000;41:4169.
[25] Platé NA, Shibaev VP, Petreukhin BS, Zubov YA, Kargin VA. J Polym Sci, Part A 1971;9:2291.
[26] Navas JJ, Alemán C, Muñoz-Guerras S. Polymer 1996;37:2589.
[27] Hsieh HWS, Post B, Morawetz HJ. Polym Sci, Polym Phys Ed 1976;14:1241.
[28] Weiner SJ, Kollman PA, Case DA, Singh UC, Ghio C, Alagona G, Profeta S, Weiner PJ. Am Chem Soc 1984;106:765.
[29] Weiner SJ, Kollman PA, Nguyen DT, Case DA. J Comput Chem 1986;7:230.
[30] de Pablo JJ, Laso M, Suter UW. J Chem Phys 1992;96:2395.
[31] Siepmann JI, Frenkel D. Mol Phys 1992;75:59.
[32] León S, Alemán C, Escalé F, Laso MJ. Comput Chem 2001;22:162.
[33] Veith WR, Tam PM, Michael AS. J Colloid Interface Sci 1966;22:360.
[34] Wang T, Heermann DW, Heilig J-C. Macromol Theory Simul 2000;9:687.
[35] van der Vergt NFA. Macromolecules 2000;33:3153.
[36] Zanuy D, Namba AM, León S, Alemán C, Muñoz-Guerra S. Polymer 2001;42:281.
[37] Platé NA, Shibaev P, Petrukhin BS, Zubov YA, Kargin VA. J Polym Sci, Pt A-1 1971;9:2291.
[38] Zanuy D, Alemán C, Laso M, Muñoz-Guerra S. J Comput Chem 2003;24:770.
[39] Widom BJ. Phys Chem 1982;86:869.
[40] Widom BJ. Chem Phys 1963;39:2808.
[41] Cuthbert TR, Wagner NJ, Paulaitis ME. Macromolecules 1997;30:3058.
[42] Toi K, Morel G, Paul DR. J Appl Polym Sci 1982;27:2997.
[43] Nosé SJ. Chem Phys 1984;81:511.